



HAL
open science

SEED: AN OPERATIONAL NUMERICAL TOOL FOR DOSIMETRIC RECONSTRUCTION IN CASE OF RADIOLOGICAL OVEREXPOSURE

Fabrice Entine, Guillaume Garnier, Matthieu Dondey, Yassine Rizzi, Antoine Gobert, Celine Bassinet, Sylvain Papin, Isabelle Pennacino, Alain Cazoulat, A Padilla, et al.

► To cite this version:

Fabrice Entine, Guillaume Garnier, Matthieu Dondey, Yassine Rizzi, Antoine Gobert, et al.. SEED: AN OPERATIONAL NUMERICAL TOOL FOR DOSIMETRIC RECONSTRUCTION IN CASE OF RADIOLOGICAL OVEREXPOSURE. Health Physics, 2022, 122 (2), pp.271-290. 10.1097/HP.0000000000001483 . hal-03525470

HAL Id: hal-03525470

<https://hal.science/hal-03525470>

Submitted on 19 Jan 2022

HAL is a multi-disciplinary open access archive for the deposit and dissemination of scientific research documents, whether they are published or not. The documents may come from teaching and research institutions in France or abroad, or from public or private research centers.

L'archive ouverte pluridisciplinaire **HAL**, est destinée au dépôt et à la diffusion de documents scientifiques de niveau recherche, publiés ou non, émanant des établissements d'enseignement et de recherche français ou étrangers, des laboratoires publics ou privés.



Distributed under a Creative Commons Attribution - NonCommercial 4.0 International License

**SEED: AN OPERATIONAL NUMERICAL TOOL FOR DOSIMETRIC
RECONSTRUCTION IN CASE OF EXTERNAL RADIOLOGICAL
OVEREXPOSURE**

F. Entine^{1,2}, G. Garnier², M. Dondey², Y. Rizzi¹, A. Gobert¹, C. Bassinet¹, S. Papin²,
I. Pennacino², A. Cazoulat², J.C. Amabile³, C. Huet¹

¹ Institute for Radiation Protection and Nuclear Safety (IRSN)

31 avenue de la Division Leclerc – 92260 FONTENAY-AUX-ROSES (France)

² French Defense Radiation Protection Service (SPRA)

1 bis rue du lieutenant Raoul Batany – CS500 – 92141 CLAMART Cedex (France)

³ Armed Forces Medical Service Head Quarter (DCSSA)

60 boulevard du général Martial Valin – CS 21 623 – 75509 PARIS Cedex 15 (France)

Corresponding author: Fabrice ENTINE, MD. Email: entinef@hotmail.com

ABSTRACT

In the event of a radiological accident involving external exposure of one or more victims and potential high doses, it is essential to know the dose distribution within the body, in order to sort the victims according to the severity of the irradiation, and then to take them to the most suitable medical facilities. However, there are currently few techniques that can be rapidly deployed on field and capable of characterizing an irradiation.

Therefore, a numerical simulation tool has been designed. It can be implemented by a doctor / physicist pairing, projected within a limited time as close as possible to the irradiation accident and emergency response teams. Called SEED (Simulation of External Exposures & Dosimetry), this tool dedicated to dose reconstruction in case of external exposure allows a rapid modeling of the irradiation scene and a visual exchange with the victims and witnesses of the event. The user can navigate in three dimensions in the accident scene thanks to a graphical user interface including a “first person” camera.

To validate the performance of the SEED tool, two dosimetric benchmarking exercises were performed. The first consisted in comparing the dose value provided by SEED to that given by a reference calculation code: MCNPX. The purpose of the second validation was to perform an experiment irradiating a physical dummy equipped with dosimeters and to reconstruct this irradiation using SEED. These two validation protocols have shown satisfactory results with mean difference less than 2% and 12% for the first and second exercises respectively. They confirm that this new tool is able to provide useful information to medical teams in charge of dosimetric triage in case of a major external exposure event.

INTRODUCTION

Given industrial, military, scientific and terrorist activities, there is a possibility of radiological accident occurring. Protocol for triage of exposed people, that sorts them into appropriate categories for treatment, is necessary. In case of external exposure, aside from the total whole-body dose, it is also essential to know the dose distribution within the body. This dosimetric estimate is based on a tripod: clinical dosimetry (**Laroche et al. 2014**), biological dosimetry (**Ainsbury et al. 2014, Kulka 2014**) and physical dosimetry (**Trompier et al. 2011**). Most of the analysis performed with biological or physical dosimetry is done in a laboratory implying a delay between the accident and the result of the dosimetry sort. Indeed, there are currently only few techniques that can be deployed in the field that are capable of rapidly characterizing an irradiation (**Sproull and Camphausen, 2016**).

Clinical dosimetry is based on the observation of the early-phase radiation-induced signs, depending on whether the irradiation is global or localized. In both cases, the early signs make it possible to carry out an initial sorting (**IRSN 2003; Dörr et al. 2017**). The earlier the first signs appear, the higher the level of exposure.

The interaction of ionizing radiation with biological systems results in a wide range of responses at the molecular and cellular levels. Biological dosimetry is based on the quantification of these responses. Several biodosimetry techniques are currently available (ICRU 94 2020). The kinetics of the blood formula is still a standard despite a monitoring period which may be too long (**REAC/TS 2013**). The most established ones are based on the radiation-induced DNA

damage and mis-repair, like the frequency of “dicentric” chromosomes and micronuclei in circulating lymphocytes (**Ainsbury et al. 2014**).

In the event of external accidental exposure, physical dosimetry cannot only be based on the emergency analysis of individual dosimeters because most of the victims do not wear any. To overcome this difficulty, several physical dosimetry techniques have been developed to assess the dose on materials collected on the victims (biological samples or materials coming from objects carried on them), used then as fortuitous dosimeters. These techniques are commonly known as “retrospective dosimetry”. Electronic Paramagnetic Resonance (EPR) allows the study of radio-induced free radicals in certain biological materials, e.g. dental enamel (**Romanyukha et al. 2014**), bone tissue (**Trompier et al. 2011**), nails (**Trompier et al. 2014**), or artificial materials e.g. glasses (**Fattibene et al. 2014**), plastics (**Trompier et al. 2011**), while luminescence-based methods can provide a dose assessment by measuring the light emitted by the materials contained in mobile phones: electronic components with thermoluminescence (TL) and optically stimulated luminescence (OSL) (**Bassinat et al. 2014, Ademola and Woda 2017**) or glasses with TL (**Discher and Woda 2013**). The delay between collecting the sample and providing the result differs from one technique to another. This delay is strongly linked to the capacity of the laboratories: a European network (RENEB) has been set up to overcome this difficulty (**Trompier et al. 2017**). In addition to these techniques and despite of a longer delay, the dosimetric reconstruction can give information on the dose distribution, experimentally using anthropomorphic phantoms equipped with dosimeters (**Huet et al. 2008**), or numerically using calculation codes mostly based on Monte-Carlo techniques (**Huet et al. 2009, Courageot et al. 2010**).

However, this dosimetric tripod has gaps. First of all, several teams give the “golden 24 hours” as decisive in initiating some specific treatments (**Farese et al. 2014**), nevertheless this requirement can’t be achieved with most of the current techniques. Clinical dosimetry only

provides information on the dose received several hours or days after irradiation depending on the time to onset of signs. Regarding biological dosimetry and retrospective physical dosimetry, on one hand, processing capacities are limited and, on the other hand, for some techniques (counting chromosomal aberrations for example), the analysis time is quite long (**Multibiodose 2013**). Then, with clinical, biological and retrospective dosimetry, it is difficult to have information about dose distribution within the body; this information is important in case of non-uniform external exposure. Finally, the reliability of dose estimation depends on the clinical signs and on the testimony of the witnesses for clinical dosimetry and numerical dose reconstruction respectively. However, some signs are not specific to irradiation and may, for example, be the result of stress caused by reports of a suspected irradiation (“worried well”) (**Stone FP 2007**). For dosimetric reconstruction, the longer the time between the accident and the simulation, the more the testimonies lose reliability and precision.

Therefore, to address these issues, a numerical simulation tool based on modern dose calculation technologies and capable of reinforcing the current diagnostic arsenal has been designed in the framework of collaboration between the French defense radiation protection service (SPRA) and the Institute for radiation protection and nuclear safety (IRSN). SEED (Simulation of External Exposures & Dosimetry) is a numerical dosimetric reconstruction software restricted to internal use (SPRA and IRSN). The aim of this tool using Geant4 Monte-Carlo code is to provide dose estimates capable of supporting the triage decisions made by specialized medical teams in case of external exposure. Its strength is also to be able to operate in a degraded situation; integrated into a militarized and hardened device, it is a stand-alone tool in terms of both power supply and simulations thanks to a powerful multi-core computer. This tool can be implemented by a doctor / physicist pair, projected within a limited time as close as possible to the irradiation accident and emergency response teams.

To validate the performance of the SEED tool, two dosimetric protocols were followed. The first protocol (validation step 1) consisted in comparing the dose value provided by SEED to that given by MCNPX Monte-Carlo code (reference calculation code usually used at IRSN in the context of accidental exposures) for identical geometric configurations, with the same number of simulated particles. The second protocol (validation step 2) aimed at comparing the reconstruction performed with SEED with an external exposure carried out under the conditions of a realistic accident that was simulated experimentally.

This paper aims to present the SEED tool as well as the validation process of the tool.

MATERIALS AND METHODS

- Dosimetric tool
 - Mobile computer

The mobile numerical tool is autonomous for its computing capacity: it does not require data transfer to a remote cluster. The computer used is based on a variant of the "Dell Precision® R7910 Workstation". Its main operating system is a Linux distribution. The computing station has 36 cores, allowing 72 simultaneous operations (hyper-threading) this ensures a greater number of operations in a shorter time. The design basis was intended to address potential requirements of processor, memory, graphics and storage.

In order to ease and to secure its transportation and use on the ground all this equipment was built-in into a military durable polyethylene container. The computer is securely attached to an aluminum chassis, itself suspended thanks to eight anti-vibration mounts. Thereby, there is an

optimal shock absorption and an efficient cooling by natural circulation of the surrounding air flow.

- SEED software

SEED is dedicated to the numerical dosimetric reconstruction of external exposure. Its main features are:

- to model an irradiation accident situation, called “scene”, from the graphical user interface (GUI);
- to generate an input file in GATE format (**Rodrigues et al 2004, Sarrut et al. 2014, Jan et al. 2011**) containing all the necessary information (geometry, physical parameters, etc.) and to launch the calculation;
- to display the results of Monte-Carlo calculations as coloured layers that can be superimposed on the elements of the scene;
- to save / load a scene;
- to create an exposure scenario combining different scenes.

SEED is programmed in C++ language and offers an interface based on an OpenGL 3D display in order to achieve a rapid modelling of the accident scene. The GUI allows the user to access all the SEED features (**Fig. 1**). By default, two monitors are used. Developed using Qt-3D[®] by an external developer (SymAlgo Technologies), this interface provides the construction of the 3D scene in a simple, precise, fast and intuitive way. The 3D scene control window (FCS3D) is located in the middle of the GUI. It is the main portal for the user to interact with the code. It includes a representation of the surrounding environment called “world” (a box large enough to include all volumes involved in the simulation) and of all the objects of the simulation scene.

Regarding objects, different volume shapes are available, from simple ones, such as box or sphere, to more advanced ones such as tessellated anthropomorphic phantoms.

The FCS3D can also include as several coloured layers a representation of calculated absorbed doses, uncertainties, number of collisions, etc. The user can move around in the FCS3D in all directions thanks to a “first person camera”. All the objects part of the scene can be easily selected with the mouse.

Moreover, objects can also be selected from the 2D scene control windows (FCS2D). These three windows correspond to 3D projections of the scene in one of the three orthogonal planes of the simulation. Any modification that is made on an FCS (2D or 3D) is instantly displayed on the other FCS.

SEED includes object parameter windows (FPO) to define the characteristics of objects part of the scene: position, size, material, etc. From the FPO, it is also possible to assign some properties to the object: irradiation source or detector which allows to interact with the simulation via the collection of information during the simulation (dose, energy deposited and/or number of collisions in a given volume).

From the GUI it is also possible to launch a Monte-Carlo calculation corresponding to the modelled scene. Then it automatically creates the input file in GATE format. To reduce the simulation time, the user can also allocate the calculation over several cores and define the number of cores. Only one calculation per scene is allowed, but it is possible to create a new scene from the elements of a previously modelled scene that has been saved. This calculation can be computed in the background while the user can work on the modelling or analysis of other scenes simultaneously. Thus, a scene can have three different status, which can be viewed on the icon relating to the scene: calculation in progress, calculation completed, design (no calculation launched).

- Calculation code

SEED uses the Geant4-based GATE (Geant4 Application for Tomographic Emission) version 8 Monte-Carlo platform to simulate the interaction between radiation and matter. GATE was originally dedicated to SPECT / PET applications and radiotherapy-brachytherapy. On the same model as Geant4-Qt, GATE development collaborators have created GATE-Qt, which allows visualizing the source, the detectors and the path of particles as well as their interaction with matter (ray-tracing) in a 3D volume.

Launching a calculation with SEED allows the creation of an input file in GATE format (.mac.), including several data:

- the definition of the "world" (dimensions and composition with materials from the GATE library: GateMaterials.db);
- the definition of the volumes which are inside the "world", characterized by a name, a position in space, dimensions, material and colour (for 3D display);
- the list of physical interactions and corresponding physical models ("physics list") which are taken into account for the Monte-Carlo simulation;
- the definition of the detector volumes and the type of expected results with the GATE simulation (dose and associated uncertainty, deposited energy, number of collisions);
- the definition of the source of ionizing radiation (nature of the particles emitted, volume or point source/isotropic or not/monoenergetic or polyenergetic);
- the parameters of the calculation (number of simulated particles, seed at the origin of the generation of random numbers).

- Validation step 1: comparison with the MCNPX calculation code

- Protocol

The objective was to benchmark the SEED tool in order to assess its accuracy and its performances. Numerical simulations were carried out for several irradiation configurations

with both the SEED tool and MCNPX reference calculation code (**Hendricks et al. 2008**). Then the doses estimated with the two codes were compared.

The principal aim was to check that the GATE input file automatically created by SEED was correct in terms of description of the geometry, description of the source, definition of the physics, etc. Recent radiological accidents (**IAEA 2004, 2009 and 2018**) and foreseen malevolent scenario mainly involve gamma sources. Thus, this benchmark, the first of many to come, was restricted to gamma emission.

Two types of geometries were defined to perform this benchmark: “simple” geometries and “complex” geometries (**Table 1**).

For “simple” geometries, only one volume was considered as a detector: a water or soft tissue phantom whose dimensions (10 cm × 30 cm × 30 cm) are close to the ICRU slab phantom (**ICRP, 1996**). These geometries principally aimed at detecting geometric configurations that could cause modelling or calculation errors in the SEED software. Therefore, several parameters were modified (source energy, source-detector distance, composition of the slab phantom, etc). Combining all these parameters, in total, 87 absorbed doses were assessed.

The number of source particles simulated for these “simple” geometries was defined so as to obtain less than 3% statistical uncertainty on the dose result. These “simple” geometries have been numbered from 1 to 4.

For “complex” geometries, a simple anthropomorphic phantom made up of 9 rectangular water volumes was designed. Thus, it was possible to estimate the heterogeneity of the dose within the body by assessing the absorbed dose in these 9 volumes defined as detectors. These “complex” geometries have been arranged to mimic accidents that occurred in the past or hypothetical accidents representing a large number of potential victims. The number of source particles simulated for these “complex” geometries has been defined so as to obtain less than

10% statistical uncertainty on the dose result. 4 “complex” geometries have been modelled, numbered from 5 to 8:

- Geometry 5 was built based on the Dakar and Abidjan accidents (2006) where one of the victims had been standing for several hours near a source hidden in a parcel (**Clairand et al. 2008**). The source was stuck in a projection tube of a radiography device. In this geometry, a spherical source (5 mm radius) of Cesium-137 (662 keV) was placed inside a wooden box next to its lead container. Two positions of the parcel were modelled: on the floor and at 1 m from the ground. Consequently, 18 absorbed doses were assessed (9 for each source position).
- Geometry 6 was constructed based on the Yanango accident (Peru, 1999) where a worker found a radiography source dropped from a radiography device on a construction site before putting it in his pants pocket (**IAEA 2000**). In this geometry, a cylindrical source of Iridium-192 in a steel capsule was placed at three positions: back pocket of the pants, hand of the victim, and front pocket of the pants. 27 (3×9) absorbed doses were calculated.
- Geometry 7 was constructed by imagining a malevolent act in a subway train with 8 victims (6 seated and 2 standing). In this geometry, a spherical source (1 cm radius) of Cobalt-60 was placed at three different positions under the seat of one of the victims. 216 ($8 \times 9 \times 3$) absorbed doses were assessed.
- Geometry 8 was constructed by imagining a terrorist act in a stadium stand containing 35 seated victims. In this geometry, a spherical source (1 cm radius) of Cobalt-60 was placed under the seat of one of the spectators. Thus, 315 (35×9) absorbed doses were assessed.

The modelling of a scene was the initial stage of this benchmark. The geometries have been defined in MCNPX and SEED with exactly the same parameters. To ensure this, the display

tools available in the two applications were used: in 2D for MCNPX and in 3D for SEED (Fig. 2).

- MCNPX: reference calculation code

MCNPX (Monte-Carlo N-Particle eXtended) is a Monte-Carlo computer code for the interaction of radiation with matter developed with FORTRAN programming language in Los Alamos from version 4c of the MCNP code (Hendricks et al. 2008). It is used by IRSN for the numerical dosimetric reconstruction in case radiological accidents (Huet et al. 2009). Version 2.6 was used as a reference for the benchmark of SEED software.

- Physics list

Before comparing the SEED software with the MCNPX calculation code, it was necessary to ensure that the two software programs used the same models for simulating the interactions of ionizing radiation with matter, in particular for photons and electrons that were the only particles transported in the calculations performed in this study.

The energy range defined by default in MCNPX (from 1 keV to 100 MeV, for both photons and electrons) has been set in SEED. Although some physics lists are already available in Geant4 (e.g., the “emstandard_opt3” constructor, that is commonly used in the medical field), it was decided at the design of the SEED software to be able to control the physical models and their parameters to be used in the simulations. This allows some interactions to be selected according to the time allowed for the simulation as well as the required degree of precision. By default, only common interactions are taken into account in SEED:

- for photons: the photoelectric effect, the Compton scattering and the pair production;
- for electrons: ionization, multiple scattering and Bremsstrahlung radiation.

In MCNPX, it is possible to add modes corresponding to the particles which have to be transported. Once these modes are defined, the physics list can be defined. However, in each mode, it is difficult to modify the different physical phenomena. Therefore, it was chosen for this validation to keep the default parameters of this calculation code, and additional physical interactions have been added to SEED: Rayleigh scattering, de-excitation by Auger electron emission, fluorescence and PIXE ("particle-induced X-ray emission").

- Validation step 2: comparison with experimental dosimetry

- Protocol

The objective was to perform experimentally the irradiation of a physical dummy equipped with dosimeters and to reconstruct this irradiation using SEED. To do this, the steps followed were:

- development of an experimental protocol;
- dummy irradiation according to the defined protocol;
- modeling, using the SEED tool, of the irradiation configuration;
- dose measurements by thermoluminescence and comparison with calculated doses obtained with SEED.

The experimentation carried out for this validation step consisted in the use of an industrial radiography source placed on the ground near an anthropomorphic physical dummy (simulating a victim) (**Fig. 3**). The ATOM CIRS[®] anthropomorphic physical phantom (detailed in the next section) was equipped with thermoluminescent dosimeters and placed about 1 m from the source on a very thin PVC holder, considered to be radio-transparent. The ATOM CIRS[®] dummy containment system consists of two plates of unknown composition. In order to obtain information on the attenuation of this plate and to characterize it as accurately as possible,

thermoluminescent dosimeters were positioned to obtain input and output measurements of the incident beam on a similar plate located on the ground at 1 m from the source.

Six parallelepiped water slabs (25 cm × 25 cm × 15 cm or 30 cm × 30 cm × 15 cm) were also used to simulate the presence of additional victims. Three of them were placed on PVC holders identical to that of the ATOM CIRS[®] phantom (locations P1 to P3) in order to simulate a seated position whereas the three others were placed on a tripod in order to simulate a standing position (locations S1 to S3). Each slab was equipped with an OSL dosimeter and a thermoluminescent dosimeter, both placed side by side in the middle of the slab front face. Finally, seven additional pairs of OSL and thermoluminescent dosimeters were placed on radio-transparent masts in order to provide information on ambient dosimetry (locations T1 to T7).

The source used for this experiment, provided by the company “Institut de Soudure Group”, was an Iridium-192 source of 2.43 TBq (activity given with an uncertainty of 10%) used for industrial radiography. The source was placed on the ground and was used without collimator in order to obtain an isotropic source emission.

The irradiation was carried out for four hours at the Beynes military camp on July 4, 2019 thanks to the collaboration of the company “Institut de Soudure Group” (**Fig. 4**).

- ATOM CIRS[®] dummy

The ATOM CIRS[®] anthropomorphic dummy measures 97.5 cm in height representing a 1.73 m tall man having a mass of 73 kg. This dummy is made of materials with the same radiological properties, in terms of energy deposition, as those found in humans. It is made up of an envelope of soft tissue, a skeleton, a brain, lungs, bone marrow and cartilage. It consists of 39 sections 2.5 cm thick in which cylindrical holes are present. These holes are placed in order to represent

the average position of 22 radiosensitive internal organs. A lookup table indicates, for each organ, the number of dosimeters to insert and the hole ID number for each inserted dosimeter.

In this experiment, all the holes belonging to an organ (271 locations) were filled with thermoluminescent dosimeters. In addition, a pair of thermoluminescent and OSL dosimeters was placed on the chest of the dummy.

- Thermoluminescence dosimetry

The thermoluminescent dosimeters used, were powder of lithium fluoride, type ${}^7\text{LiF:Mg,Cu,P}$ (GR207). The powder was packaged in cylindrical plastic tubes (2.5 cm high and 5 mm in diameter). The 287 LiF dosimeters placed on the scene (271 in the dummy, 1 on the dummy chest, 6 on the water slabs, 7 to measure ambient dose and 2 on the holder plate) were read by thermoluminescence technique (TL). Blue TL measurements were performed with a Fimel reader (France) and annealing with a Fimel oven (France). Conditions were as follows: pre-irradiation annealing at 240°C for 10 min, post-irradiation preheat at 135°C for 15 s and heat up to 240°C at a heating rate of 3°Cs⁻¹. The TL signals of the tubes were measured within fifteen days of the irradiation. In addition, the powder was stored at a stable temperature and was protected from light, so the signal loss could be ignored.

Each tube contained enough powder for four to five readings. It was chosen to carry out three thermoluminescence measurements per tube, except in the event of significant dispersion of the latter (standard deviation/average>5%) or the presence of a dose gradient within the tube. In these cases, a fourth measurement was carried out. Around 1000 measurements were performed in total, each lasting approximately two minutes.

The calibration curve was performed after the irradiation at the IRSN's medical linear accelerator “Elekta Synergy[®] Platform”. Eleven powder tubes dedicated to the calibration were

irradiated in air kerma from 10 mGy to 2.5 Gy with a 4 MV photon beam. As Iridium-192 energy differs from the calibration energy, a correction factor was determined. The main gamma rays of Iridium-192 are emitted at 468 keV (48%), 316 keV (83%), 308 keV (29%) and 296 keV (28%). A unique correction factor of 0.98 (+/-5%) corresponding to the mean Iridium-192 energy (367 keV) was used.

Depending on the location of the dosimeter, different dose quantities were assessed: absorbed dose in the material for dosimeters in the CIRS dummy, $H_p(10)$ for dosimeters placed on the water slabs and on the dummy, air kerma for the dosimeters placed on the masts and on the holder plate.

For the determination of the conversion factors, once again, Iridium-192 energy was approximated by its mean energy.

Regarding organ doses, SEED calculates an energy deposited in the material considered, Therefore, for the dosimeters inserted in the dummy, air kerma was converted to absorbed dose in the material (tissue, brain, lung or bone) by applying coefficients from the literature (**Hubbel and Seltzer 2004**).

In order to compare the doses measured on the slabs and on the ATOM CIRS[®] dummy by the two types of dosimeters expressed in air kerma and $H_p(10)$ for LiF and OSL respectively, the air kerma values obtained with the thermoluminescent dosimeters were converted into $H_p(10)$. The conversion factor for air kerma into $H_p(10)$ was established using the data supplied by the International Commission on Radiation Units & Measurements (**ICRU 1998**). The conversion factor for air kerma/ $H_p(10)$ obtained for 367 keV was 1.316 (+/- 9.70%).

An uncertainty budget was performed (**Table 2**). Then uncertainty for thermoluminescent measurements was evaluated using error propagation as described in GUM (**ISO 2008**). It takes into account: the reproducibility of the measurements performed with the powder of the same

tube, the uncertainty on the calibration, the uncertainty due to the difference in response of the LiF dosimeters between the calibration energy and the energy of the Iridium-192 and the uncertainty on the conversion factor from air kerma into kerma in the material or $H_p(10)$. Regarding the uncertainty on the dosimeter calibration, it takes into account the uncertainty on the calibration coefficient of the ionization chamber used (given on the calibration certificate) and the uncertainties on every correction coefficient applied (recombination, temperature, pressure, polarity).

The average dose to the organ was estimated by calculating the average of the doses obtained from the tubes assigned to this organ. A calculation of the coefficient of variation between the tubes of the same organ made it possible to notice the presence of a dose gradient within this organ. Uncertainty on the average organ dose was assessed by applying the propagation of uncertainties described in GUM from the uncertainty of each tube belonging to the organ.

- Optically stimulated luminescence dosimetry

Radiation dose was also measured with aluminum oxide doped with carbon ($Al_2O_3:C$) detectors read out by optically stimulated luminescence (OSL). OSL dosimeters were read by the SPRA dosimetry laboratory and were similar to passive dosimeters used to monitor workers exposed to ionizing radiation under normal working conditions.

The readers of OSL dosimeters were calibrated with irradiated dosimeters on ISO phantom in a gamma radiation beam of Cesium-137. Dosimeters were irradiated by an independent and accredited laboratory. The calibration curve was established between 0.10 mSv and 10 Sv. Finally, the radiation dose was evaluated with a dose estimation algorithm. The doses assessed with these dosimeters were expressed in individual dose equivalent $H_p(10)$ for dosimeters on

the water slabs and on the dummy. For the other locations, it was converted into air kerma thanks to the conversion factor determined as described above.

- Integration of mesh objects in SEED

The experimental validation consists in comparing the results of the numerical simulation with those obtained with the OSL and LiF dosimeters. It therefore requires a representation of the scene as close as possible to reality. In order to minimize the dose differences between simulations and measurements, it was decided to use a numerical phantom generated from the CT images of the ATOM CIRS[®] dummy. An ad hoc procedure was developed in order to create MESH objects from DICOM format images and to implement this format in SEED.

A mesh object is a three-dimensional object made up of vertices, edges and faces organized in polygons. This type of object only describes the geometry of the surface of an object. Mesh objects allow resolution as fine as desired by increasing the number of polygons of the object.

The following procedure was adopted:

- Use of 3DSlicer[®] software to convert the DICOM[®] format images into a mesh (**Fedorov et al. 2012**)
- Export of this mesh in .STL (STereo-Lithography) format according to the coordinates system created by 3DSlicer;
- Use of Meshlab[®] software in order to convert the binary STL file generated by 3DSlicer into an ASCII STL file. This software also provides the reduction of the number of mesh vertices while keeping its geometry. In order to limit the use of the resources of the computing station when displaying geometries, the number of vertices of the different

meshes is reduced before their integration into SEED, taking care not to alter their geometric quality.

- STL ASCII file upload in SEED and mesh display.
 - Mesh volume calculation in order to be able to calculate the dose from the energy deposited in the mesh volume.
-
- Modeling of the irradiation scene with SEED

The ATOM CIRS[®] physical dummy was scanned at the military Percy Hospital. It had 399 cross sections 2.5 mm apart, and was saved in DICOM format. The images were imported into 3DSlicer[®] and the volumes corresponding to structures of the dummy whose physical density is different from that of the soft tissue were created using the 3DSlicer's contrast contouring tool: brain, bone, lungs, marrow and cartilage. This technique made it possible to create bodies of geometry identical to those present in the ATOM CIRS[®] dummy. The other parts of the dummy were soft tissue equivalent. It was therefore necessary to create the organs manually based on the set of maps provided by the manufacturer showing the hypothetical outline of the internal organs appropriate for each section. (**Fig. 5**). The holes that are drilled into each section are also shown on the map along with the corresponding unique hole ID number. The map was used in conjunction with the lookup table mentioned previously.

To create these “virtual” organs, the contours of the organs were manually drawn on each section in 3DSlicer. The volume corresponding to the organ was then created by the software by extrapolating between the different sections previously outlined. Next the geometric shape of the organs was adjusted manually using an anatomical atlas, to give them a shape closer to reality. The ATOM CIRS[®] dummy represents a man (1.73 m; 73 kg) whose dimensions are very close to these of the ICRP 110 reference male voxel phantom (1.76 m; 73 kg). Therefore,

the volumes of its organs were manually corrected so as to approximate those of the ICRP 110 reference male phantom (**ICRP 2007**). Finally, a smoothing of the external contour was carried out in order to eliminate the roughness and to make the organs geometrically more realistic (**Fig. 6**). Moreover, 8 LiF tubes, evenly distributed within the phantom, were modeled as a mesh in order to allow one-to-one dose comparisons.

The 3D volumes generated by 3DSlicer had a very high spatial resolution, far beyond our dosimetric reconstruction needs. The files were therefore very large, so they were compressed by reducing the number of vertices to 5% of the initial number, and this for all objects (except the eight LiF tubes modeled), in order to obtain a good compromise between the file size and the accuracy of geometry. In order to validate the phantom construction procedure, the center of the various organs was compared with the theoretical center of the organs of the ATOM CIRS[®] dummy provided by the manufacturer. The materials of the ATOM CIRS[®] dummy were also added to the GATE materials list (**Table 3**). The volumes therefore have the same composition under SEED as in reality. The only exception is the cartilage at the ends of the ribs, the density of which is not defined by the manufacturer. It was then chosen to use the material of the intervertebral discs because of their close density, verified on the CT images.

The other objects of the irradiation scene were modeled by simple geometries. The surrounding volume (world), 15 m × 15 m × 5 m, had a 50 cm thick box over its entire surface (**Fig. 7**) representing the soil of the experiment (material equivalent to the soil defined in the GateMaterials.db file).

LiF dosimeters placed outside the dummy were modeled using cylinders 2.5 cm high with a radius of 0.25 cm arranged vertically, and composed of soft tissue. The OSL dosimeters were represented by vertical boxes of 7.3 cm × 3.5 cm × 1 cm composed of air. These two types of dosimeters were considered as detectors in SEED. The slabs were represented by two sizes of

vertical boxes made up of water: 25 cm × 25 cm × 15 cm and 30 cm × 30 cm × 15 cm. The PVC holders, on which the ATOM CIRS® dummy and the slabs are placed, were not modeled because of their radio-transparency. Likewise, the masts supporting some dosimeters were also not modeled.

The dummy's holder plates were modeled by two rectangular parallelepipeds, made of PVC, 18.8 cm × 1.9 cm × 32 cm for the lower plate and 17 cm × 1.9 cm × 30 cm for the upper plate. The additional plate used to calculate the attenuation of these was represented by a PVC rectangular parallelepiped of 15 cm × 1.9 cm × 20 cm.

The activity of the Iridium-192 source given by the supplier was in fact not the real activity of the 10 iridium-192 pellets but calculated from the dose rate measured with the encapsulated source. It was therefore not possible to perform the simulation with the faithful modeling of the encapsulated source, even if the geometry was perfectly known. This is why this encapsulated source has been defined by a point source, surrounded by 2 thicknesses of stainless steel: the source holder and the cannula (**Fig. 8**).

Energy deposition in the material composing the different objects was computed by GATE and converted by SEED to absorbed dose taking into account the mass of the objects. The physics list used was the same as the one used in the first validation. Finally, in order to obtain a low statistical uncertainty, 10^{11} particles were simulated. The calculation, launched on 28 cores, lasted nearly four days.

RESULTS

- Validation step 1: comparison with the MCNPX calculation code
 - Dose comparison

A summary of the results for the different configurations is shown in **Table 4**. For each geometry, the mean relative difference between SEED and MCNPX calculated from all the calculated absorbed doses assessed for the considered geometry is given. In addition, the mean relative difference was also estimated for the 4 simple (87 absorbed doses assessed) and the 4 complex (576 absorbed doses assessed) geometries and for all the 663 calculated absorbed doses (simple + complex geometries). Regarding the eight geometries, the mean relative difference ranges from 0.40% (geometry 2) to 2.83% (geometry 8). The overall mean relative dose difference between the two calculation codes is around 2%. Differences are a bit larger for complex geometries (2.14%) than for simple geometries (1.55%).

- Dose layer

The comparison between SEED and MCNPX was based on the numerical values of the mean absorbed doses calculated in the different detection volumes with the two codes. These results were collected in the output files for each code. SEED also allows direct display of the dose distribution on the scene using 3D and 2D dose layers (**Fig. 9**). This feature is particularly useful for “complex” geometries with a large number of victims.

- Validation step 2: comparison with experimental dosimetry
 - Doses measured by thermoluminescence

The coefficient of variation (CV) within a tube, defined as the ratio of the standard deviation to the mean, obtained from the 287 thermoluminescent dosimeters is 4.7% with a variation

between 0.2% and 12.4%. Only the tube placed on the farthest slab phantom (location P1) shows greater CV (35.8%).

The absorbed doses in the material where the tube is inserted obtained for the 271 tubes in the dummy range from 45.2 mGy to 1.73 Gy, with uncertainties between 7.19% and 14.4% (1σ). For the tubes placed on the masts the air kerma ranges from 14.2 mGy to 1.44 Gy, with uncertainties between 5.15% and 14.8% (1σ). Finally the $H_p(10)$ obtained for the other tubes (placed on the slabs and on the chest of the ATOM CIRS[®] dummy) range from 1.49 mSv to 300 mSv with uncertainties between 13.8% and 16.3% (1σ), except for the dosimeter located on slab P1: 46.7%.

The average organ absorbed doses range from 72.6 mGy (left shoulder) to 1.73 Gy (right testicle) (**Fig. 10**). Uncertainties are around 10% (1σ). The CV within the tubes belonging to the same organ ranges from 4% (heart, 2 tubes) to 100% (left costal grill, 9 tubes). A large dispersion is also observed for the brain (82%, 4 tubes).

- Doses measured by optically stimulated luminescence

The dose quantities (air kerma or $H_p(10)$) obtained by thermoluminescence for the dosimeters placed outside the phantom were compared with the dose quantities (air kerma or $H_p(10)$) obtained by OSL (**Fig. 11**). The relative difference is less than 10% for all dosimeters, except for three locations: chest of the CIRS[®] dummy [$H_p(10)$] (159%), T7 (21%) and P1 [$H_p(10)$] (24%).

- Doses calculated by SEED

In order to ease the comparison between the doses calculated by SEED and the measured doses, results were divided into three groups: the doses relating to the elements located outside the CIRS[®] phantom, the average doses to the organs of the CIRS[®] dummy and the doses

corresponding to 8 thermoluminescent dosimeters distributed in the CIRS[®] phantom and individually modeled in mesh format in SEED. The results are presented in **Table 5**, **Table 6**, and **Fig. 12** respectively.

Regarding the elements located outside the CIRS phantom, the relative difference between calculated and measured dose ranges from 0.1% (LiF P2) to 170% (OSL P1). The average relative difference is 24% considering all the dosimeters and falls to 11.60% if OSL P1 (170 %), LiF P1 (128 %), OSL CIRS (20 %) and LiF CIRS (87 %) are excluded (see discussion section). For the other dosimeters located outside the anthropomorphic dummy, considering the confidence intervals, no significant difference is observed between measured and calculated doses except for LiF and OSL dosimeters located in T3 (34 % and 32% respectively).

The relative difference between calculated and measured organ doses is 11.7% on average and ranges from 0.09 % (left costal grill) to 43.28 % (right scapula). Considering the confidence intervals, no significant difference is observed between measured and calculated doses except for 6 among 39 organs; left and right scapula (43%), cervical spine (26%), lumbar and thoracic spine (25%), skull (27%) and right femur (20%).

Finally, a good agreement is obtained between measured and calculated doses for the 8 thermoluminescent dosimeters distributed within the ATOM CIRS[®] phantom: the mean relative difference is 5.4% (variation between 0.7% for tube 29 in the thyroid and 21.3% for tube 9 in the left part of the brain).

DISCUSSION

- Validation step 1: comparison with the MCNPX calculation code

Due to the targeted uncertainties for the simulations (less than 3% for “simple” geometries and less than 10% for “complex” geometries), a very good agreement was obtained between the two methods with a relative difference average of around 2% for "simple" and "complex" geometries. Nevertheless, “complex” geometries greatly contribute to increase this mean relative deviation. Indeed, “complex” geometries have a relative difference of 2.14% compared to 1.55% for “simple” geometries (**Table 4**). This higher value for "complex" geometries is explained by the large number of volumes involved and the presence of volumes of small dimensions and sometimes located far from the source (feet of the victims), which implies significant uncertainty. As the relative dose difference is directly linked to statistical uncertainty, it can be assumed that simulating a much larger number of particles (unreasonable in terms of calculation time for a real application of the SEED tool) would have made it possible to reduce significantly the average relative dose difference for “complex” geometries.

This study has revealed that modeling was simpler and faster with SEED than with MCNPX, in particular if the time of preparing the input file is also included. This observation is not surprising, because SEED is a dedicated software that allows modeling the majority of the scene only with the mouse, thanks to the graphic interface that facilitates the 3D vision of the scene whereas MCNPX is a generalist Monte-Carlo code. For MCNPX, the input file must be written entirely on the keyboard and viewing in 2D only makes the validation of the geometry more difficult. For example, the construction time of geometry 8 required more than 7 hours on MCNPX against 3 hours for SEED. However, if the geometry had been directly constructed in Geant4 (that means without any dedicated GUI), it would probably have taken as long as with MCNPX. This tool therefore shows great potential regarding this optimization of modeling time. In addition, modeling assistance features had not yet been implemented at the time of validation step 1 (copy and paste, object grouping, etc.). These tools help to increase time savings in modelling.

This validation step 1 made it possible to validate all of SEED's functionalities, from modelling the scene to reading the results of the simulations. Several methods for facilitating the readout and display of the obtained results are under development: direct access to SEED output files, tooltips on dose layers by positioning the mouse pointer on the volume or voxel concerned, digital tables integrated into the software and printable. At the time of this validation step 1, only direct reading of the output files was operational.

- Validation step 2: comparison with experimental dosimetry

First, as expected the CV within the tubes belonging to the same organ is low (<10%) for small organs where tubes are close to one another, as the prostate for instance (8% within 3 tubes). It is the same for larger organs, heart for instance, for which the mean dose is calculated from a small number of dosimeters (2 or 3) close to one another. On the other hand, regarding organs for which the mean dose has been estimated from tubes far from one another, a higher dispersion is obtained: costal grill (100% and 41% for left and right side respectively, 9 tubes) and thyroid (30%, explained by the anatomical shape of the thyroid and the use of 6 tubes spread over the two lobes) for instance.

Secondly, a good agreement is observed between the doses obtained by thermoluminescence and by OSL for the dosimeters placed outside the phantom (relative difference <10%), except for the CIRS[®] dosimeters $[H_p(10)]$, P1 $[H_p(10)]$ and T7. For CIRS[®] $[H_p(10)]$ placed on the ATOM CIRS[®] dummy, a higher dose (+159%) was obtained with OSL dosimetry: the LiF dosimeter was placed behind the OSL dosimeter relative to the source and this difference could be explained by the masking of the LiF dosimeter by the OSL dosimeter. A second hypothesis involves the angular response of the OSL dosimeter. The P1 dosimeters were placed on the slab located 9 m from the gamma source: the difference can be explained by the large dispersion

(36%) obtained from the four measurements of the LiF tube. Indeed, the signal value measured for the farthest slab phantom LiF was close to that of the background noise of the device, which explains this large dispersion. Therefore, the values obtained for CIRS[®] [$H_p(10)$] and P1 [$H_p(10)$] were excluded from comparisons with the simulation. Regarding OSL T7, it was placed below the LiF T7 tube, on a mast located just behind the dummy, and therefore the dummy was between the source and the dosimeters. The heterogeneity of the intercalated dummy may be at the origin of the observed difference (21%). However, the materials of the dummy were faithfully modelled in SEED. Consequently, these values were not excluded from comparisons with the simulation. This hypothesis is confirmed by the good agreement obtained between measurements and calculations on one hand for OSL T7 (9.4%) and on the other hand for LiF T7 (2.8%).

On the whole, the agreement between calculated and measured doses is also good (**Table 5**, **Table 6** and **Fig. 11**). However, dose differences are obtained in some cases. Regarding the average dose to organs, the first explanation of the differences is probably related to the method of calculating this average: average of the results of the organ dosimeters for the measured dose, energy really deposited in the volume of the organ for the calculated dose. Thus, the smaller the organ is and the more dosimeters there are, the easier it is to reproduce the dose gradient within the organ. Consequently, the mean calculated absorbed dose is close to the measured one. For instance, it is the case for thyroid: although a large dispersion (30%) is observed within the six tubes belonging to this organ, the agreement between measurements and calculation is 0.4%. The good agreement obtained between measured and calculated doses on one hand for the eight dosimeters individually modelled within the phantom and on the other hand for small organs with only one dosimeter (breasts, adrenals and testes: difference below 6 %) also confirms this hypothesis.

In addition, the main differences concern bone structures: right scapula (43.28%), left scapula (42.26%), skull (26.86%), etc. In these organs, approximations may occur due to shape, size and material of dosimeters. Indeed, bones can be a thin volume, crossed by LiF dosimeters longer than the bone itself. Moreover, the skeletal anatomy of the CIRS[®] dummy includes a homogeneous bone tissue composition that averages known cortical to trabecular ratios. Its density is about 1.60, whereas the density considered for the conversion factor kerma in air/kerma in bone for the LiF dosimeters was about 1.92, corresponding to cortical bone **(Hubbel et al. 2004)**.

If we set aside the results concerning the bones, no additional organ shows a significant difference between calculated and measured doses. The average difference is then 7.41%: it is close to the average difference for the 8 dosimeters which are distributed throughout the phantom (5.43%).

Finally, concerning the duration of the simulation approaching four days, this is explained by the need to obtain a very low statistical uncertainty for this experimental validation step. Thus, a large number of particles was simulated which therefore directly increased the computation time. Obviously, this is unreasonable in terms of calculation for a real application of the SEED tool.

CONCLUSION AND PERSPECTIVES

In the case of an accident involving a large number of victims, it is necessary to perform a rapid dosimetric triage according to the severity of the exposures, in order to organize the treatment as well as possible. Recent scientific advances have made it possible to help carry out this sorting, but the numerical simulation had not yet been investigated. SEED is a dedicated tool for numerical dosimetric reconstruction. The two validation studies made it possible to test the

SEED software and to confirm the logic of the software and the ergonomics of the interface. For gamma sources, it was possible to ensure the adequacy of the results of this software based on Geant4 with the reference code (MCNPX) on the one hand, and with experimental dosimetry by thermoluminescence on the other hand.

Several works are planned (some are in progress) to improve SEED features and to go further in the validation of the tool. Thus, a "scenario" functionality will allow the objects modelled during movement to be set in time, by calculating the dosimetric summation resulting from the sequence of several static scenes. In the validation step 1, the implemented physics list only takes into account the physical phenomena for photons and electrons. In the future, it will be necessary to create a physics list for neutrons and to compare this list with that of another code. It will also be interesting to implement variance reduction features in order to save time on simulations with large scenes and volumes located far from the source.

Moreover, in the context of comparison with other computer codes, some complements and parameters could be explored. It could thus be envisaged to simulate accident scenes with several sources or even to study a dose distribution using voxelized detectors. Comparing the results with non-isotropic sources could be interesting. It is also planned to compare the results obtained using the mesh representation of the ATOM CIRS[®] dummy with a representation using a mathematical phantom. The purpose of this comparison will be to estimate the error in the dose to the various organs due to the representation of the victim by a mathematical phantom if it is not possible to use a more realistic numerical phantom. Finally, although such a validation phase 3 has not yet been defined, the simulation of an accident in the field could be considered, in a "supposedly real" situation, as part of an authentic dosimetric survey during a national nuclear security exercise.

ACKNOWLEDGMENTS

The authors would like to thank:

- The French defense procurement agency (DGA) and its defence innovation agency (AID) for the initial financing of the project.
- The company “SymAlgo Technologies” for the development of the GUI and for the fruitful discussions regarding SEED features.
- The company “Institut de Soudure Group” for having supplied the radioactive source and for having provided their assistance in carrying out the experiment in good safety conditions.
- The company “Polatom” for having communicated to us the precise technical parameters of the radioactive source.
- The French National Gendarmerie for having helped our team in organizing the gamma irradiation on its military training field.
- Dr Jocelyne Aigueperse for having initiated the collaboration between IRSN and SPRA which was at the origin of this new dosimetric tool.

REFERENCES

Ademola JA, Woda C. Thermoluminescence of electronic components from mobile phones for determination of accident doses. *Radiat. Meas*; 104: 13-21, 2017.

Ainsbury EA, Barnard S, Barrios L, Fattibene P, De Gelger V, Grégoire E, Lindholm C, Lloyd D, Nergaard I, Rothkamm K, Romm H, Scherthan H, Thierens H, Vandervoorde C, Woda C,

Wojcik A. Multibiodose radiation emergency triage categorization software. *Health Phys*; 107(1): 83-89, 2014.

Bassinet C, Woda C, Bortolin E, Della Monaca S, Fattibene P, Quattrini MC, Bulanek B, Ekendahl D, Burbidge CI, Cauwels V, Kouroukla E, Geber-Bergstrand T, Mrozik A, Marczewska B, Bilski P, Sholom S, Mckeever SWS. Retrospective radiation dosimetry using OSL of electronic components: Results of an inter-laboratory comparison. *Radiat. Meas*; 71: 475-479, 2014.

Clairand I, Huet C, Trompier F, Bottollier-Depois JF. Physical dosimetric reconstruction of a radiological accident due to gammagraphy equipment that occurred in Dakar and Abidjan in summer 2006. *Rad. Meas*; 43: 689-703, 2008.

Courageot E, Sayah R, Huet C. Development of modified voxel phantoms for the numerical dosimetric reconstruction of radiological accidents involving external sources: Implementation in SESAME tool. *Physics in Medicine and Biology*; 55(9): 231-241, 2010.

Discher M, Woda C. Thermoluminescence of glass display from mobile phones for retrospective and accident dosimetry. *Radiat. Meas*; 53-54: 12-21, 2013.

Farese AM, Brown CR, Smith CP, Gibbs AM, Katz BP, Johnson CS, Prado KL, Macvittie TJ. The ability of filgrastim to mitigate mortality following LD50/60 total-body irradiation is administration time-dependent. *Health Phys*; 106(1): 39-47, 2014.

Fattibene P, Trompier F, Wieser A, Brai M, Ciesielski B, De Angelis C, Della Monaca S, Garcia T, Gustafsson H, Hole EO, Juniewicz M, Krefft K, Longo A, Leveque P, Lund E, Marrale M, Michalec B, Mierzwioska G, Rao JL. EPR dosimetry intercomparison using smart phone touch screen glass. *Radiation and Environmental Biophysics*; 53(2):311-320, 2014.

Fedorov A, Beichel R, Kalpathy-Cramer J, Finet J, Fillion-Robin JC, Pujol S, Bauer C, Jennings D, Fennessy F, Sonka M, Buatti J, Aylward SR, Miller JV, Pieper S, Kikinis R. 3D Slicer en tant que plate-forme de traitement d'images pour le réseau d'imagerie quantitative. Imagerie par résonance magnétique; 2012. (in French).

Hendricks JS, McKinney GW, Fensin ML, James MR, Johns RC, Durkee JW, Finch JP, Pelowitz DB, Waters LS, Johnson MW. MCNP 2.6.0 Extensions. Los Alamos National Laboratory. 2008.

Hubbel JH, Seltzer JM. Tables of X-Ray Mass Attenuation Coefficients and Mass Energy - Absorption coefficients (version 1.4). Gaithersburg: National Institute of Standards and Technology (NIST). 2004.

Huet C, Trompier F, Clairand I, Queinnec F, Bottollier-Depois JF. Physical dosimetric reconstruction of radiological accident at Fleurus (Belgium) on 11 March 2006. Radiat. Meas; 43(2-6): 845-848, 2008.

Huet C, Lemosquet A, Clairand I, Rioual JB, Franck D, De Carlan L, Aubineau-Lanièce I, Bottollier-Depois JF. SESAME: A software tool for the numerical dosimetric reconstruction of radiological accidents involving external sources and its application to the accident in Chile in December 2005. Health Phys; 96(1): 76-83, 2009.

Institute for Radiation Protection and Nuclear Safety (IRSN). Indications des greffes de cellules souches hématopoïétiques et stratégie thérapeutique des irradiations accidentelles. Abbaye des Vaux-de-Cernay (Yvelines): 2003. (in French).

International Atomic Energy Agency (IAEA). The Radiological Accident in Yanango. 2000.

International Atomic Energy Agency (IAEA). The Radiological accident in Cochabamba. 2004.

International Atomic Energy Agency (IAEA). The Radiological accident in Nueva Aldea. 2009.

International Atomic Energy Agency (IAEA). The radiological accident in Chilca, Georgia. 2018.

International Commission on Radiation Units & Measurements (ICRU). Table A.24 - Conversion coefficients from air kerma free-in-air to $H_p(10,0^\circ)$ in an ICRU slab and angular dependence factors $R(10,\alpha)$. ICRU Report 57: 110, 1998.

International Commission on Radiological Protection (ICRP). Conversion coefficients for use in radiological protection against external radiation. ICRP Publication 74. Annals of the ICRP vol 26 n° 3-4. Pergamon Press, Oxford, 1996.

International Commission on Radiological Protection (ICRP). Table 5.2 List of source and target regions, their segmented volumes, and resulting masses compared with the reference masses (ICRP, 2002). ICRP Publication 110, 2007.

International Organization for Standardization (ISO). Guide to the expression of uncertainty in measurement (GUM). 2008.

Jan S, Benoit D, Becheva E, Carlier T, Cassol F, Descourt P, Frisson T, Grevillot L, Guigues L, Maigne L, Morel C, Perrot Y, Rehfeld N, Sarrut D, Schaart DR, Stute S, Pietrzyk U, Visvikis D, Zahra N, Buvat I. GATE V6: a major enhancement of the GATE simulation platform enabling modelling of CT and radiotherapy. Phys. Med. Biol; 56: 881-901, 2011.

Kulka, U. Realising the European network of biodosimetry: RENEB - Statu quo. Radiation Protection Dosimetry; 164(1-2): 42-45, 2014.

Laroche P, Gagna G, Castagnet, X, Amabile JC. Radiological hazards: treatment of radiocontaminated injured casualties. *Encyclopédie Médico Chirurgicale (EMC)*. Paris: Elsevier Masson, *Médecine d'urgence*; 8(4): 1-12, 2013. (in French).

Multibiodose. Guidance for using MULTIBIODOSE tools in emergencies. 2013.

Radiation Emergency Assistance Center/Training Site (REAC/TS). The medical aspect of radiation incidents. 2013.

Rodrigues P, Moura R, Ortigao C, Peralta L, Pia MG, Trindale A, Varela J. Geant4 Applications and Developments for Medical Physics Experiments. *Transactions on Nuclear Science*; 51(4): 1412-1419, 2004.

Romanyukha A, Trompier F, Reyes RA. Q-band electron paramagnetic resonance dosimetry in tooth enamel: Biopsy procedure and determination of dose detection limit. *Radiation and Environmental Biophysics*; 53(2):305-310, 2014.

Sarrut D, Bardies M, Boussion N, Freud N, Jan S, Letang JM, Loudos G, Maigne L, Marcatili S, Mauxion T, Papadimitroulas P, Perrot Y, Pietrzyk U, Robert C, Schaart D, Visvikis D, Buvat I. A review of the use and potential of the GATE Monte Carlo code for radiation therapy and dosimetry applications. *Med. Phys*; 41(6): 064301, 2014.

Sproull M, Camphausen K. State-of-the-Art Advances in Radiation Biodosimetry for Mass Casualty Events Involving Radiation Exposure. *Radiation Research*: 186; 423-435, 2016.

Stone FP. The "Worried Well" Response to CBRN Events: Analysis and Solutions. Counterproliferation Paper No. 40. USAF Counterproliferation Center. Air University, 2007.

Trompier F, Bassinet C, Monaca Della S. Overview of physical and biophysical techniques for accident dosimetry. *Radiation Protection Dosimetry*; 144(1-4): 571-574, 2011.

Trompier F, Romanyukha A, Reyes R, Vezin H, Queinnec F, Gourier D. State of the art in nail dosimetry: Free radicals identification and reaction mechanisms. *Radiation and Environmental Biophysics*; 53(2):291-303, 2014.

Trompier F, Burbidge C, Bassinet C, Baumann M, Bortolin E, De Angelis C, Eakins J, Della Monaca S, Fattibene P, Cristina Quattrini M, Tanner R, Wieser A, Woda C. Overview of physical dosimetry methods for triage application integrated in the new European network RENE. *International Journal of Radiation Biology*; 93(1): 65-74, 2017.

FIGURE LEGENDS

- **Table 1:** Description of the 4 “simple geometries” and 4 “complex geometries” and of source parameters used for the benchmark between SEED and MCNPX.
- **Table 2:** Evaluation of uncertainty sources for thermoluminescent measurements.
- **Table 3:** Materials constituting the ATOM CIRS[®] dummy used for modelling.
- **Table 4:** Summary of dose differences obtained between MCNPX and SEED for simple and complex geometries.
- **Table 5:** Comparison of the measured and calculated doses for elements outside the CIRS[®] dummy.
 - * Dosimeters written in italics were excluded from the calculation of the average quantities (see discussion).
- **Table 6:** Comparison of the measured and calculated doses for the CIRS[®] dummy organs.

- **Figure 1:** SEED graphical user interface with the use of 2 monitors. The GUI is composed of a 3D display (FCS3D) and a 2D display (FCS2D) of the scene and object parameter windows (FPO). A simple anthropomorphic phantom with coloured layers representing absorbed dose is displayed on the FCS3D.
- **Figure 2:** Display of geometries 7 (source in a subway train) (top) and 8 (terrorist act in a stadium) (bottom) with MCNPX (left) and SEED (right). Geometry 7: seated and standing victims are represented in green and pink on MCNPX and SEED display respectively. Geometry 8: seated victims are represented in blue and pink on MCNPX and SEED display respectively.
- **Figure 3:** Overview of the planned experimental protocol and associated expected dose rates (dose rate calculated from the specific constant of the source). The anthropomorphic CIRS physical dummy simulates a seated victim. Slabs filled with water are used to simulated other seated (P1 to P3 locations) or standing (S1 to S3 locations) victims whereas ambient dose is assessed using dosimeters placed on masts (T1 to T7 locations).
- **Figure 4:** Picture of the different items (gammagraphy projector, CIRS physical dummy representing a seated victim, water slabs representing seated and standing victims, masts equipped with dosimeters for ambient dose assessment and holder plate placed on the ground to assess its attenuation) placed on the irradiation scene.
- **Figure 5:** Example of a section map showing theoretical organ outlines together with the location and identification of the holes (on that section: liver (8 holes), spleen (4 holes), stomach (3 holes), left kidney (2 holes), adrenals (1 hole) and spine (1 hole)).

- **Figure 6:** ATOM CIRS[®] adult male phantom made up of 43 volumes, with 3DSlicer (left) and Meshlab (right).
- **Figure 7:** Overview of the experiment carried out on a military site (top) and irradiation scene modelled using SEED (bottom). On SEED display, water slabs are in blue, LiF and OSL dosimeters respectively in green and pink, the source (cannula) in red, the ground in brown and the holder plate in black.
- **Figure 8:** Modelling of the accurate geometrical source (yellow and red parts, left) and of the source as a point source (in SEED, for display needs, a point source is represented by a sphere, right). The green cylinder and the blue cylinder represent the source holder and the cannula respectively. The two white cylinders represent the air surrounding the source and the source holder. Green lines exiting from the source are the particle trajectories.
- **Figure 9:** Dose layer displayed with SEED on geometry 7 (top) and geometry 8 (bottom).
- **Figure 10:** Mean organ dose obtained from thermoluminescent dosimeters measurement (left) and CV obtained from the dosimeters belonging to the same organ (right). Error bars represent the combined standard uncertainty on mean organ dose obtained from the method described in the “Thermoluminescence dosimetry” paragraph and the sources of uncertainty specified in Table 2.
- **Figure 11:** Comparison of air kerma and $H_p(10)$ obtained with the LiF and OSL dosimeters. Relative difference is less than 10% except for P1, T7 and CIRS [$H_p(10)$]. For LiF dosimeters, error bars represent the combined standard uncertainty on air kerma or $H_p(10)$ obtained from the method described in the “Thermoluminescence dosimetry”

paragraph and the sources of uncertainty specified in Table 2. For OSL dosimeters, error bars represent the $H_p(10)$ uncertainty provided by the SPRA dosimetry laboratory. For air kerma, the uncertainty on the correction factor mentioned in table 2 was also taken into account to assess the OSL air kerma uncertainty.

- **Figure 12:** Comparison of the measured and calculated doses for the 8 dosimeters modelled in the CIRS[®] dummy. For the measurement, error bars represent the combined standard uncertainty on the kerma in the material obtained from the method described in the “Thermoluminescence dosimetry” paragraph and the sources of uncertainty specified in Table 2 while for the simulation they represent the 1-sigma statistical uncertainty.

Figure 1



Figure 2

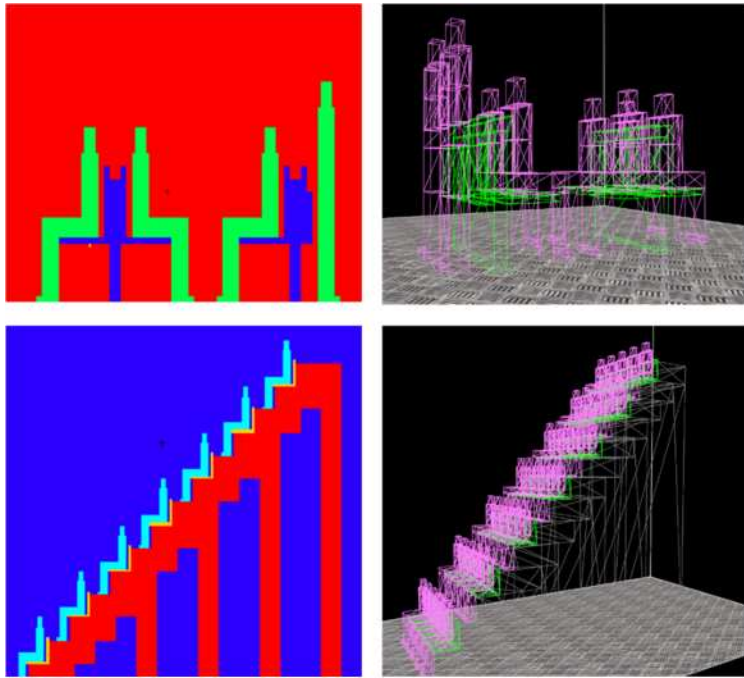


Figure 3

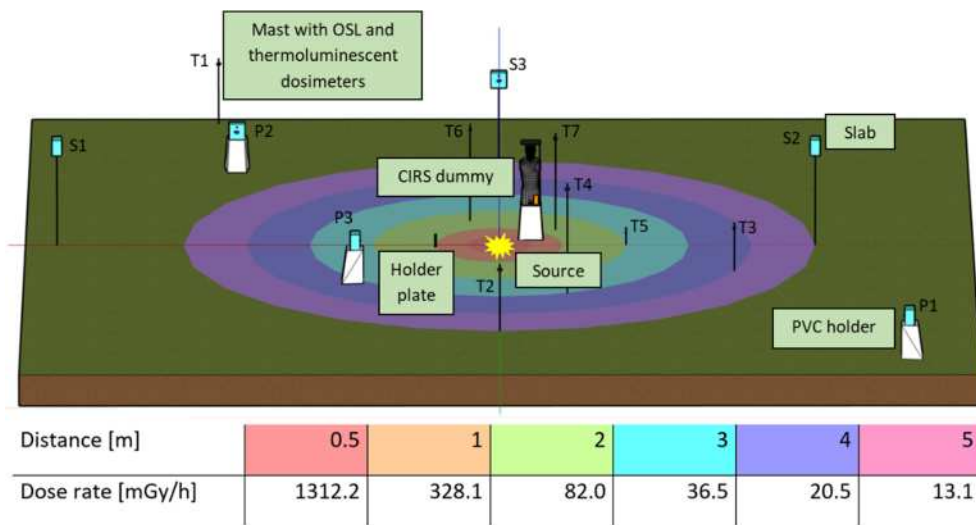


Figure 4



Figure 5

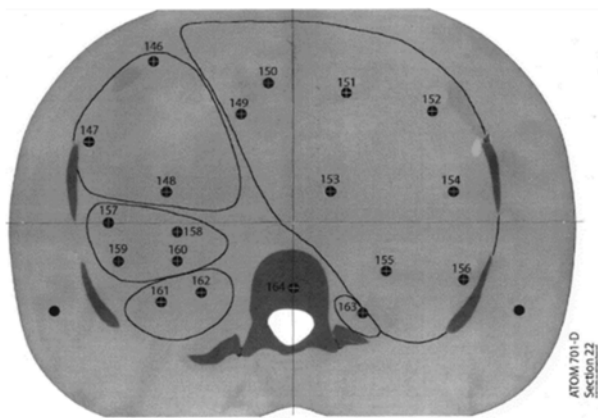


Figure 6

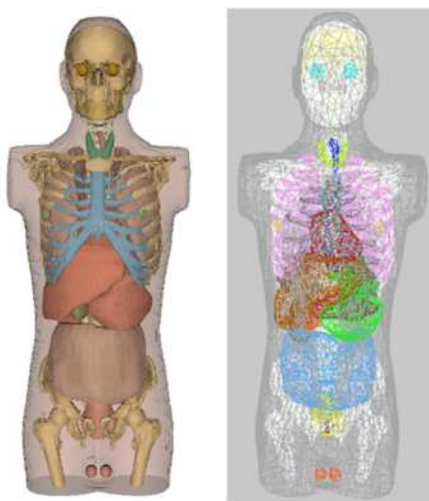


Figure 7

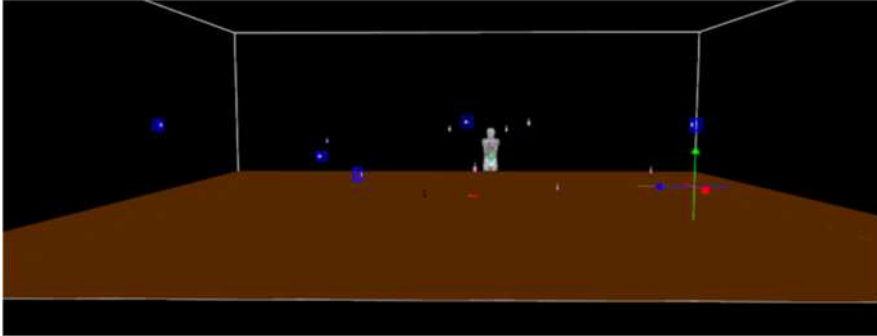


Figure 8

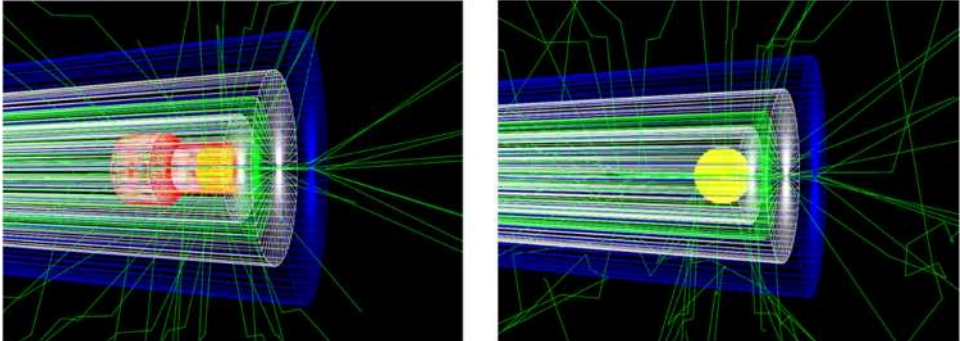


Figure 9

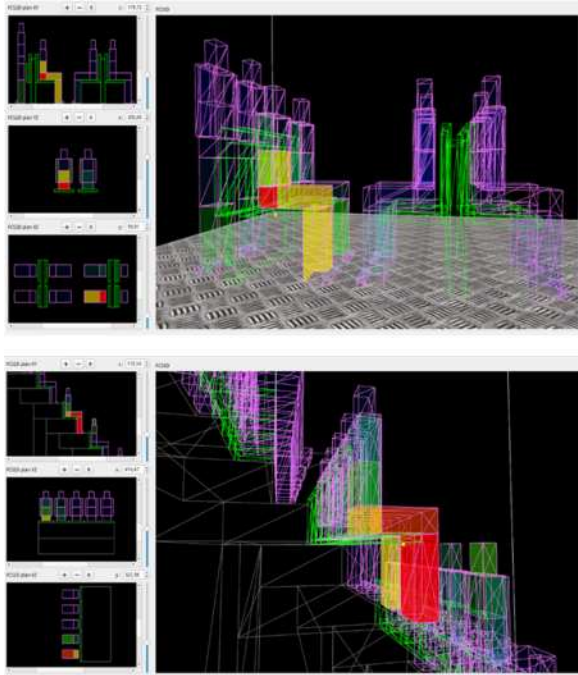


Figure 10

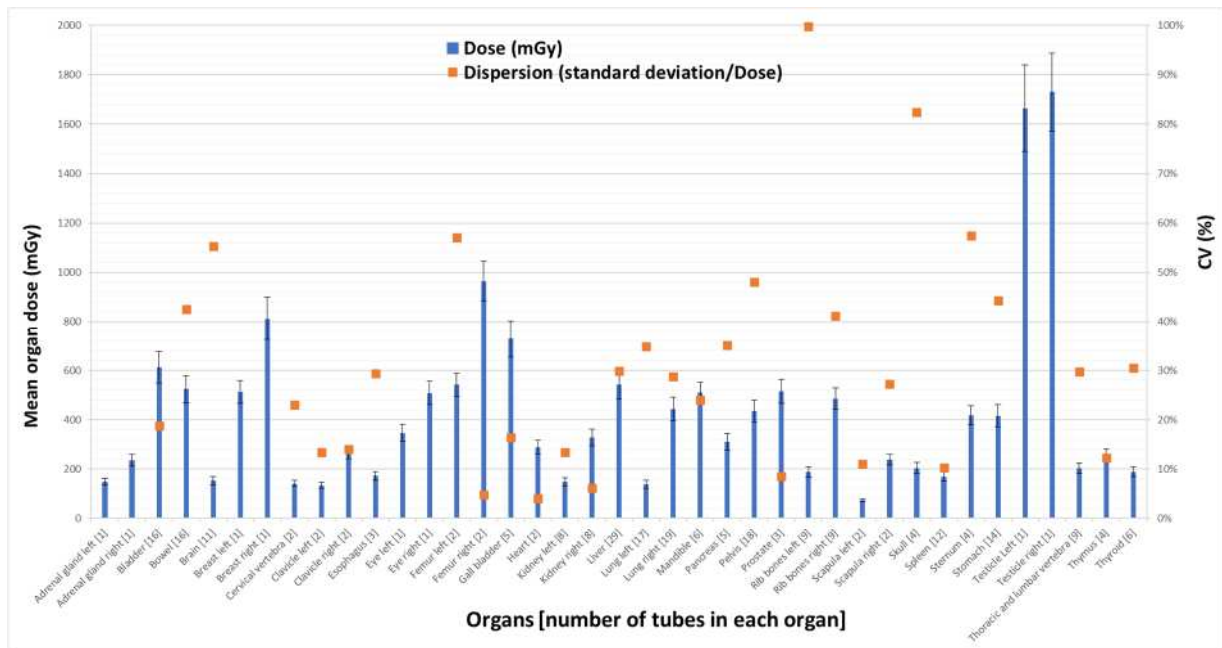


Figure 11

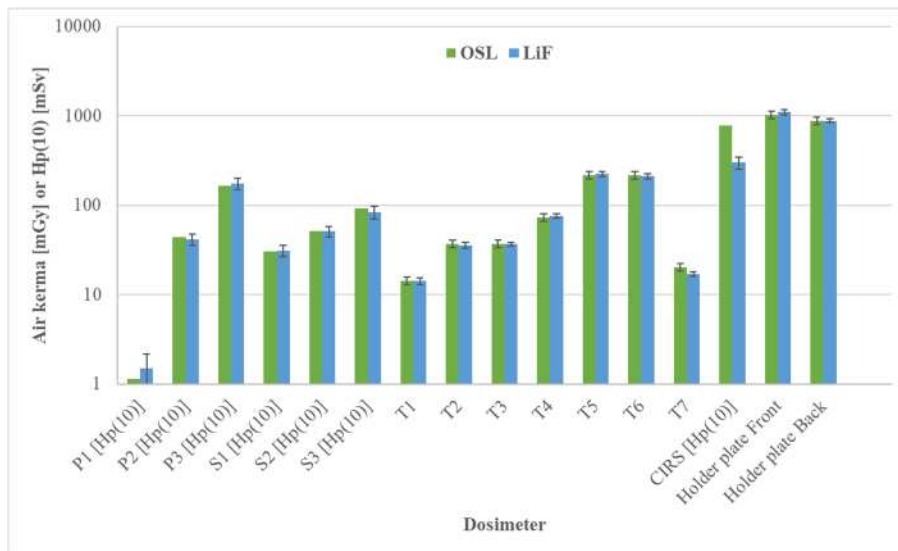


Figure 12

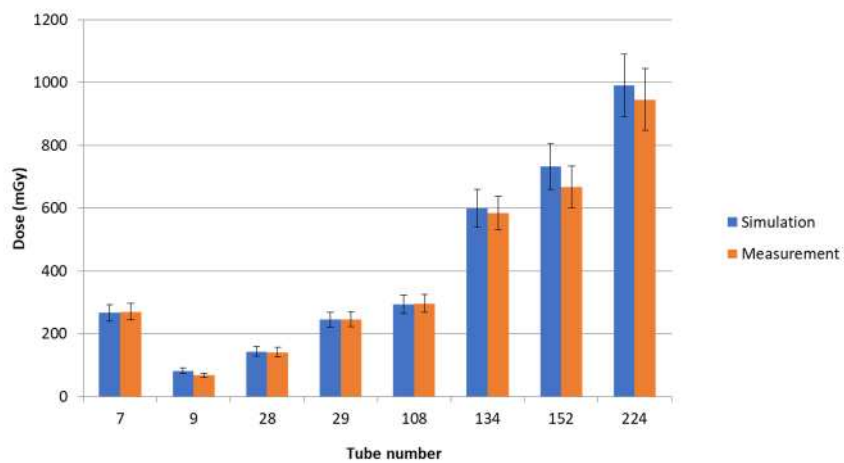


Table 1

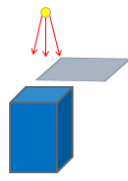
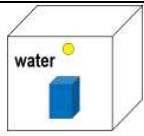
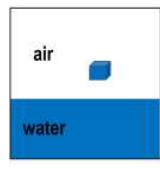
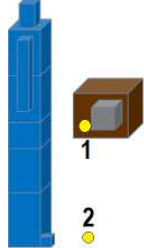
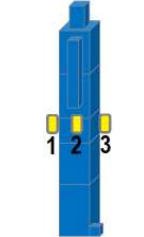
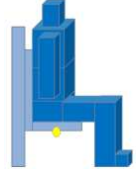
Geometry	World Composition Size	Detector	Source	Source-detector distance	Number of absorbed doses assessed	Schema
1	Air 5 m × 5 m × 5 m 10 m × 10 m × 10 m	Water volume 10 cm × 30 cm × 30 cm	⁶⁰ Co / ¹⁹² Ir Point source Spherical source Cylindrical source	2 cm 20 cm 200 cm With/with out lead screen	72	
2 Water world	Water 5 m × 5 m × 5 m	Water volume Soft tissue 10 cm × 30 cm × 30 cm	⁶⁰ Co / ¹⁹² Ir Point source Cylindrical source	2 cm 20 cm	8	
3 Contaminated water	Air 5 m × 5 m × 5 m	Water phantom 10 cm × 30 cm × 30 cm	Water volume contaminated with ⁶⁰ Co 2 m × 5 m × 5 m	5 cm	1	
4 Heterogeneous phantom	Air 5 m × 5 m × 5 m	Heterogeneous volume (Water and lung equivalent)	⁶⁰ Co point source Point source of 120 keV	30 cm	6	
5 Dakar Abidjan accidents	Air 5 m × 5 m × 5 m	9 water volumes schematically representing human body	¹³⁷ Cs spherical source	Victim's abdomen Victim's feet	18	
6 Yanango accident	Air 5 m × 5 m × 5 m	9 water volumes schematically representing human body	¹⁹² Ir cylindrical source	Back pocket In the hand Front pocket	27	
7 Subway train	Air 5 m × 5 m × 5 m	8 human bodies each composed of 9 water volumes	¹⁹² Ir spherical source	Three positions under the seat	216	
8 Stadium stand	Air 10 m × 10 m × 10 m	35 human bodies each composed of 9 water volumes	⁶⁰ Co spherical source	Under the seat	315	

Table 2

Uncertainty source ¹	Value (%)
Reproducibility of measurements	0.2 - 35.8
Dosimeter calibration ²	5
Energy response correction factor	5
Air kerma into kerma in the material correction factor ³	5.0 - 7.3
Air kerma into $H_p(10)$ correction factor ⁴	9.7
Combined standard uncertainty	5.1 - 46.7

¹ The table lists the uncertainty sources that have been identified for LiF measurements. However, depending on the final quantity to assess, some are not taken into account to estimate the combined uncertainty.

² Used only for the calibration dosimeters.

³ Used only when the final quantity to assess is kerma in the material.

⁴ Used only when the final quantity to assess is $H_p(10)$.

Table 3

	Elements (%)									Density (g/cm^3)
	C	O	H	N	Ca	P	Mg	Cl	Al	
Bone	0.359	0.346	0.047	0.009	0.148	0.028	0.060	0.000	0.000	1.60
Soft tissue	0.574	0.246	0.084	0.016	0.000	0.000	0.076	0.001	0.000	1.05
Spinal cord	0.542	0.266	0.073	0.021	0.000	0.000	0.093	0.002	0.000	1.07
Intervertebral	0.462	0.308	0.067	0.018	0.000	0.000	0.140	0.002	0.000	1.15
Lungs	0.633	0.204	0.083	0.031	0.000	0.000	0.000	0.013	0.032	0.21
Brain	0.536	0.265	0.081	0.015	0.000	0.000	0.099	0.001	0.000	1.07

Table 4

Geometries	Number of calculated absorbed doses	Mean statistical uncertainty (both SEED and MCNPX) (%)	Mean relative dose difference (%)
1	72	0.90	1.72
2	8	0.15	0.40
3	1	1.00	0.97
4	6	0.75	1.18
5	18	1.15	1.27
6	27	0.55	1.09
7	216	1.15	1.33
8	315	1.90	2.83
Sub-total "simple"	87	0.87	1.55
Sub-total "complex"	576	1.50	2.14
Total	663	1.40	2.06

Table 5

Dosimeter	Calculated dose (mGy)	Calculated dose standard deviation (mGy)	Measured dose: $H_p(10)$ or air Kerma (mGy)	Measured dose standard deviation (mGy)	Deviation from measured dose (%)
<i>OSL P1*</i>	3.05	0.72	1.13	0.19	169.89
OSL P2	31.38	4.67	43.89	7.49	28.49
OSL P3	137.86	19.52	165.93	28.30	16.92
OSL S1	28.05	4.23	30.66	5.23	8.50
OSL S2	50.73	7.38	51.9	8.85	2.26
OSL S3	75.25	10.81	91.69	15.64	17.93
OSL T1	12.30	1.52	14.31	2.81	14.09
OSL T2	39.75	4.29	36.95	7.25	7.58
OSL T3	49.06	5.23	37.15	7.29	32.05
OSL T4	86.49	8.97	73.12	14.35	18.28
OSL T5	239.36	24.25	217.05	36.44	10.28
OSL T6	235.38	23.87	216.10	36.28	8.92
OSL T7	22.35	2.57	20.42	4.01	9.43
<i>OSL CIRS*</i>	617.42	86.31	776.93	106.43	20.53
<i>LiF P1*</i>	3.40	0.61	1.49	0.69	128.18
LiF P2	41.45	6.62	41.49	5.78	0.1
LiF P3	178.86	28.20	176.2	25.33	1.51
LiF S1	28.57	4.58	31.07	4.49	8.04
LiF S2	57.53	9.13	50.97	7.05	12.87
LiF S3	86.95	13.75	83.74	13.66	3.84
LiF T1	13.13	1.73	14.19	1.17	7.47
LiF T2	40.68	5.13	35.79	2.87	16.67
LiF T3	49.05	6.17	36.67	1.89	33.77
LiF T4	84.83	10.58	76.13	3.93	11.43
LiF T5	244.06	30.26	223.11	15.24	9.39
LiF T6	222.81	27.63	212.37	14.7	4.92
LiF T7	13.37	2.21	16.9	0.96	2.81
<i>LiF CIRS*</i>	560.09	88.09	299.68	44.37	86.90
LiF holder plate	1040.63	128.68	1101.18	67.01	5.5
Overall average (P1 and CIRS excluded)	124.56	15.68	123.96	13.52	11.60

Table 6

Organ	Calculated average absorbed dose (mGy)	Calculated average dose standard deviation (mGy)	Measured average absorbed dose (mGy)	Measured average dose standard deviation (mGy)	Deviation from measured absorbed dose (%)
Brain	153.05	15.31	151.93	17.91	0.74
R. clavicle	299.68	29.97	266.42	23.65	12.48
L. clavicle	155.14	15.52	133.86	11.78	15.90
Heart	315.67	31.57	288.45	27.73	9.44
R. costal grill	492.54	49.25	484.16	43.67	1.73
L. costal grill	188.40	18.84	188.24	20.41	0.09
Skull	258.09	25.81	203.44	22.01	26.86
Stomach	465.72	46.57	415.40	45.04	12.12
R. Femur	1163.40	116.34	964.41	80.28	20.63
L. Femur	626.56	62.66	541.51	48.05	15.71
Liver	576.41	57.64	542.03	59.10	6.34
Intestine	618.52	61.85	524.05	55.77	18.03
Mandible	577.25	57.73	510.66	41.69	13.04
R. eye	478.46	47.85	508.59	46.47	5.92
L. eye	286.15	28.62	346.27	34.23	17.36
Esophagus	201.59	20.16	172.24	17.06	17.04
Pancreas	327.15	32.72	309.76	33.60	5.62
Pelvis	525.27	52.53	435.00	42.87	20.75
R. lung	469.86	46.99	443.50	47.33	5.94
L. lung	157.20	15.72	137.47	15.61	14.35
Prostate	520.22	52.02	515.89	48.49	0.84
Rate	184.49	18.45	169.11	17.21	9.09
R. kidney	365.22	36.52	328.55	33.42	11.16
L. kidney	161.45	16.15	148.60	16.18	8.65
R. scapula	341.88	34.19	238.61	20.84	43.28
L. scapula	103.34	10.33	72.64	6.35	42.26
R. breast	820.27	82.06	812.69	86.85	0.93
L. breast	487.78	48.82	512.33	46.32	4.79
Sternum	446.01	44.60	417.40	39.72	6.85
R. adrenal gland	227.82	22.79	236.05	23.19	3.48
L. adrenal gland	156.27	15.64	147.47	13.76	5.97
R. testicle	1818.76	181.88	1729.80	156.23	5.14
L. testicle	1662.04	166.21	1664.66	174.74	0.16
Thymus	287.09	28.71	256.67	25.28	11.85
Thyroid	188.22	18.83	188.99	20.43	0.41
Cervical spine	177.7	17.77	141.39	11.94	25.68
Lumbar & thoracic spine	255.03	25.50	203.71	21.34	25.19
Gallbladder	776.40	77.64	729.08	74.49	6.49
Bladder	592.46	59.25	612.55	63.99	3.28
Average for all organs	459.19	45.92	428.04	41.92	11.68